THERAPEUTIC POTENTIALS OF HYPOXIC- AND BAICALEIN-ENRICHED FRACTION-PRECONDITIONED HUMAN NEURAL STEM CELLS FOR *IN VITRO* ISCHEMIC STROKE MODEL

KANG IN NEE

UNIVERSITI SAINS MALAYSIA

2018

THERAPEUTIC POTENTIALS OF HYPOXIC- AND BAICALEIN-ENRICHED FRACTION-PRECONDITIONED HUMAN NEURAL STEM CELLS FOR *IN VITRO* ISCHEMIC STROKE MODEL

by

KANG IN NEE

Thesis submitted in fulfillment of the requirements

for the degree of

Doctor of Philosophy

April 2018

ACKNOWLEDGEMENTS

On the successful completion of this project, I would like to express my sincere gratitude to my main supervisor, Dr. Tan Suat Cheng for her scientific guidance throughout the experimental work and continuous encouragement during the writing of this thesis.

Heartfelt thanks to my co-supervisor, Prof. Dr. Shaharum Shamsuddin for providing the equipment, cell lines and reagents for molecular work. Thank you for the advice and support throughout my studies. I would also like to express my gratitude to my co-supervisor, Dr. Lee Chong Yew for accepting me to conduct part of my research in his laboratory. Thank you for helping me out during the difficult times, for sharing his vast knowledge of phytochemistry and chromatography. It was a pleasant opportunity to work with him.

I am very grateful to all former and present lab members from molecular biology and cell culture laboratories for their help and time throughout my study. I would also like to thank Associate Prof. Dr. See Too Wei Cun and his postgraduate students for sharing chemicals, equipment and knowledge during my difficult times. In addition, I would also like to show my gratitude to all lab members from Prof. Chan Kit Lam's laboratory for sharing their knowledge, experiences, equipment and solvents throughout my work in USM Penang. On top of that, I would also like to extend my gratitude to all the great peoples I have met along the way, particularly to my former colleagues from Cancer Research Initiatives Foundation (CARIF). They have developed my research, analytical and problem solving skills during my 3 years of

tenure with the organisation. Thank you for the friendship and memories.

Furthermore, I am also grateful to the Ministry of Higher Education Malaysia for providing financial aid via MyBrain15 studentship and Research University Individual (RUI) Grant (Grant no: 1001/PPSK/812140). Besides that, I am very grateful to Next Gene Scientific Sdn. Bhd. for allowing me to use the demo unit of CytoSMART^{TM} Lux 2 for a month.

Last but not least, my deepest gratitude goes to my late father who passed away from intracranial hemorrhage, for his continuous encouragement. I always knew that he believed in me and wanted the best for me. Also to my mother and sisters, who have been accompanying me throughout my postgraduate studies. Thank you for staying up late with me in the laboratory while I worked late. The journey would not have been possible without their support.

TABLE OF CONTENTS

Acknowledgements ii

Table of Contents iv

List of Tables xvii

List of Figures xix

List of Symbols, Abbreviations and Acronymns xxvii

Abstrak xxxiii

Abstract xxxv

CHAPTER 1 : INTRODUCTION 1

1.1 Stroke 1

1.1.1 Pathophysiologic cascades in ischemic stroke 3

1.1.1(a) Energy failure 3

1.1.1(b) Ionic imbalance 6

1.1.1(c) Glutamate excitotoxicity 8

1.1.1(d) Inflammation 10

1.1.1(e) Free radical production 10

1.1.2 Reperfusion injury 13

1.1.3 Current treatment for stroke 13

1.1.4 Stem cell therapy 14

1.2 Preconditioning strategy 17

1.2.1 Hypoxic preconditioning 18

1.2.2 Pharmacological preconditioning by baicalein-enriched fraction 18

1.2.2(a) Baicalein-enriched fraction from *Oroxylum indicum* 19

1.2.3 Preconditioning-induced neuroprotective signaling 22

1.2.3(a) Hypoxia-inducible factor-1 alpha (HIF-1α) 22

1.2.3(b) Neurogenic locus notch homolog protein 1 (Notch 1) 27

1.2.3(c) Vascular endothelial growth factor A (VEGFA) 30

1.2.3(d) Angiopoietin-1 (ANGPT1) 33

1.2.3(e) Nuclear factor erythroid 2-related factor 2 (Nrf2) 36

1.2.3(f) Sodium dismutase 1 (SOD1) 39

1.3 Best reference gene 41

1.3.1 β-actin (*ACTB*) 41

1.3.2 Eukaryotic initiation factor 4A (*eIF4A*) 42

1.3.3 Glyceraldehyde-3-phosphate dehydrogenase (*GAPDH*)……...42

1.3.4 Hypoxanthine phosphoribosyl transferase 1 (*HPRT1*)…….....43

1.3.5 Importin 8 (*IPO8*)…….. ..... .43

1.3.6 Peptidyl-prolyl isomerase A (*PPIA*) ..... .43

1.3.7 Ribosomal protein L13A (*RPL13A*) ..... .44

1.3.8 60S ribosomal protein large P1 (*RPLP1*) 44

1.3.9 TATA box binding protein (*TBP*) ..... .44

1.3.10 Tyrosine 3-monooxygenase/tryptophan 5- monooxygenase activation protein, zeta polypeptide (*YWHAZ*) 45

1.4 Rationale of the study ..... .45

1.5 Aims of the study 47

1.5.1 General aim 47

1.5.2 Specific aims 47

1.6 Overview of the study 48

CHAPTER 2 : GENERAL MATERIALS AND METHODS 49

2.1 Materials 49

2.1.1 General instruments 49

2.1.2 General consumables 49

2.1.3 Chemicals and reagents 49

2.1.4 Antibodies 49

2.1.5 Primers 49

2.1.6 Software 49

2.1.7 Kits 60

2.1.8 Cell lines 60

2.1.8(a) H9-derived human neural stem cell (H9-hNSCs) 60

2.1.8(b) Human neuroblastoma cell (SH-SY5Y) 60

2.2 Preparation of media, buffers and solutions 61

2.2.1 Preparation of cell culture medium and solutions 61

2.2.1(a) All-*trans* retinoic acid (ATRA) 61

2.2.1(b) Recombinant human brain-derived neurotrophic factor (BDNF) 61

2.2.1(c) Recombinant human basic fibroblast growth factor (bFGF) 61

2.2.1(d) Recombinant human epidermal growth factor (EGF) 61

2.2.1(e) 1X Phosphate-buffered saline (PBS) 62

2.2.1(f) Complete Stempro® NSC serum free medium (SFM) 62

2.2.1(g) Astrocyte medium 62

2.2.1(h) Neuronal medium 62

2.2.1(i) Complete SH-SY5Y growth medium 63

2.2.1(j) 2X Freezing medium 63
2.2.2 Preparation of coating matrix 63
2.2.2(a) Poly-D-lysine hydrobromide (PDL) 63
2.2.3 Preparation of solutions for agarose gel electrophoresis 64
2.2.3(a) Ethidium bromide (EtBr) solution 64
2.2.3(b) Tris-acetate-EDTA (TAE) buffer 64
2.2.4 Preparation of solutions for sodium dodecyl sulfate polyacrylamide gel electrophoresis (SDS-PAGE) 64
2.2.4(a) 4X Separating buffer 64
2.2.4(b) 4X Stacking buffer 64
2.2.4(c) 6X Sample loading buffer 65
2.2.4(d) 10% (w/v) Ammonium persulfate (APS) 65
2.2.4(e) 10X Tris-glycine SDS running buffer 65
2.2.5 Preparation of solutions for western blotting 66
2.2.5(a) SDS transfer buffer 66
2.2.5(b) 10X Tris-buffered saline (TBS) 66
2.2.5(c) TBS-Tween washing buffer (TBST) 66
2.2.5(d) Blocking solution 1 66
2.2.5(e) Blocking solution 2 67
2.2.5(f) Ponceau S solution 67
2.2.5(g) Mild stripping buffer 67
2.2.6 Preparation of solutions for immunocytochemistry (ICC) 67
2.2.6(a) 20% (w/v) Paraformaldehyde (PFA) fixative stock solution 67
2.2.6(b) 4% (v/v) PFA fixative solution 68

2.2.6(c) Permeabilization solution 68
2.2.6(d) ICC blocking solution 68
2.3 General methods 68
2.3.1 Cell culture 68
2.3.1(a) Culture vessel coating with CELLstart™ CTS™ 68
2.3.1(b) Thawing H9-hNSC 69
2.3.1(c) Passaging H9-hNSC 70
2.3.1(d) Freezing H9-hNSC 70
2.3.1(e) Culture vessel coating with fibronectin 71
2.3.1(f) Thawing SH-SY5Y 71
2.3.1(g) Passaging SH-SY5Y 72
2.3.1(h) Freezing SH-SY5Y 72
2.3.1(i) Tetrazolium (MTT) assay 73
2.3.2 Reverse transcription and quantitative real-time PCR (qPCR) 74
2.3.2(a) RNA extraction 74
2.3.2(b) DNase treatment 75
2.3.2(c) Determination of RNA integrity 76
2.3.2(d) Complementary DNA (cDNA) synthesis 77
2.3.2(e) Primer design and optimization 77
2.3.2(f) Gradient PCR amplification 78
2.3.2(g) Agarose gel electrophoresis 78
2.3.2(h) Primer efficiency test 79
2.3.2(i) Quantitative real-time PCR (qPCR) 80
2.3.3 Data analysis 81
2.3.3(a) Stability of reference genes 81

2.3.3(b) Quantitation of target gene expression 84
2.3.4 Western blot 85
2.3.4(a) Protein lysate preparation 85
2.3.4(b) Determination of protein concentration 85
2.3.4(c) Sodium dodecyl sulfate-polyacrylamide gel electrophoresis (SDS-PAGE) 86
2.3.4(d) Gel apparatus assembly 86
2.3.4(e) Preparation of separating gel (10%) 87
2.3.4(f) Preparation of stacking gel (4%) 87
2.3.4(g) Sample preparation and loading 88
2.3.4(h) Transfer of protein 88
2.3.4(i) Detection and band quantitation 89
2.3.4(j) Stripping for re-probing 90
2.3.5 Immunocytochemistry (ICC) 91
2.3.5(a) Coverslip preparation and coating 91
2.3.5(b) Coverslip coating with PDL/laminin 91
2.3.5(c) Coverslip coating with Geltrex® 92
2.3.5(d) Coverslip coating with fibronectin 92
2.3.5(e) Fixing and permeabilizing cells 93
2.3.5(f) Blocking and staining cells 93
2.3.5(g) Fluorescence imaging 94
2.3.6 Statistical analysis 95
2.3.7 Hypoxic preconditioning of H9-hNSCs 95
2.3.8 Plant specimen of *Oroxylum indicum* (*O. indicum*) 95
2.3.9 Preparation of crude extract from *O. indicum* leaves 96

2.3.10 Preparation of baicalein-enriched fraction from *O. indicum* crude extract 97
2.3.11 Thin layer chromatography (TLC) 99
2.3.12 Ultraviolet (UV) visible absorption spectra 100
2.3.13 High performance liquid chromatography (HPLC) 101

CHAPTER 3 : HYPOXIC PRECONDITIONING OF H9-HNSC AND ITS NEUROPROTECTIVE POTENTIAL 103
3.1 Introduction 103
3.1.1 Aims of work 104
3.1.2 Overview of this chapter 105
3.2 Methods 106
3.2.1 Determination of the best preconditioning duration 106
3.2.1(a) Assessment of cell proliferation and viability 106
3.2.1(b) Assessment of hypoxia-inducible factor-alpha (HIF-1α) and nestin protein expression 106
3.2.2 Assessment of differentiation potential of hypoxic-preconditioned H9-hNSCs 107
3.2.2(a) Astrocyte differentiation potential 107
3.2.2(b) Neuronal differentiation potential 108
3.2.2(c) Immunocytochemistry (ICC) 108
3.2.3 Assessment of neuroprotective potentials of hypoxic-preconditioned H9-hNSCs 109
3.2.3(a) Best reference gene selection 109
3.2.3(b) Neuroprotective gene expression 109

3.3 Results 110
3.3.1 Effects of hypoxic preconditioning on proliferation and viability of H9-hNSCs 110
3.3.2 Effects of hypoxic preconditioning on HIF-1α and nestin protein expression in H9-hNSCs 113
3.3.3 Effects of hypoxic preconditioning on astrocyte differentiation potential of H9-hNSCs 118
3.3.4 Effects of hypoxic preconditioning on neuronal differentiation potential of H9-hNSCs 122
3.3.5 Best reference genes selection for normoxic- and hypoxic-preconditioned H9-hNSCs 126
3.3.5(a) RNA purity and integrity 126
3.3.5(b) PCR amplification specificity and efficiency for candidate reference genes 128
3.3.5(c) Expression level of candidate reference genes 133
3.3.6 Expression stability of candidate reference genes 135
3.3.6(a) Reference gene ranking based on geNorm 135
3.3.6(b) Reference gene ranking based on NormFinder 138
3.3.6(c) Reference gene ranking based on BestKeeper 140
3.3.6(d) Comprehensive ranking of candidate reference genes 144
3.3.7 Neuroprotective signaling of hypoxic preconditioning on H9-hNSCs 146
3.3.7(a) PCR amplification specificity and efficiency for target genes 146
3.3.7(b) Relative quantification of target genes 151

3.4 Discussion 153
3.4.1 Hypoxic preconditioning for 24 h promoted H9-hNSC proliferation 153
3.4.2 Hypoxic preconditioning upregulated HIF-1α and nestin expression in H9-hNSCs 153
3.4.3 Hypoxic preconditioning promoted astrocyte and neuronal differentiation of H9-hNSCs in the absence of growth factors 154
3.4.4 *RPLP1* and *RPL13A* as the best reference gene for normoxic- and hypoxic-preconditioned H9-hNSCs 155
3.4.5 Upregulation of neuroprotective and paracrine effects following hypoxic preconditioning 157
3.5 Conclusion 162

CHAPTER 4 : BAICALEIN-ENRICHED FRACTION PRECONDITIONING OF H9-HNSC AND ITS NEUROPROTECTIVE POTENTIAL 163
4.1 Introduction 163
4.1.1 Aims of work 164
4.1.2 Overview of this chapter 165
4.2 Methods 166
4.2.1 Preconditioning of H9-hNSCs using baicalein-enriched fraction 166
4.2.2 Determination of the best parameters for preconditioning 166
4.2.2(a) Assessment of cell proliferation and viability 166
4.2.3 Assessment of differentiation potential of H9-hNSCs preconditioned with baicalein-enriched fraction 167
4.2.3(a) Astrocyte differentiation potential 167

4.2.3(b) Neuronal differentiation potential 167
4.2.3(c) Immunocytochemistry (ICC) 168
4.2.4 Assessment of neuroprotective potentials of H9-hNSCs preconditioned with baicalein-enriched fraction 168
4.2.4(a) Best reference gene selection 169
4.2.4(b) Neuroprotective gene expression 169
4.3 Results 170
4.3.1 Yield of crude extract 170
4.3.2 Enrichment of baicalein via fractionation 170
4.3.3 Determination of baicalein by TLC 170
4.3.4 Determination of best UV absorption for HPLC 173
4.3.5 Quantification of baicalein by HPLC 173
4.3.6 Effects of F5 preconditioning on proliferation and viability of H9-hNSCs 179
4.3.7 Effects of F5 preconditioning on astrocyte differentiation potential of H9-hNSCs 182
4.3.8 Effects of F5 preconditioning on neuronal differentiation potential of H9-hNSCs 186
4.3.9 Best reference genes selection for control and F5-preconditioned H9-hNSCs 190
4.3.9(a) RNA purity and integrity 190
4.3.9(b) Expression level of candidate reference genes 192
4.3.10 Expression stability of candidate reference genes 194
4.3.10(a) Reference gene ranking based on geNorm 194
4.3.10(b) Reference gene ranking based on NormFinder 197

4.3.10(c) Reference gene ranking based on BestKeeper 199
4.3.10(d) Comprehensive ranking of candidate reference genes ... 202
4.3.11 Neuroprotective signaling of F5 preconditioning on H9-hNSCs..... 204
4.3.11(a) Relative quantification of target genes 204
4.4 Discussion 206
4.4.1 Baicalein-enriched fraction, a promising pharmacological agent..... 206
4.4.2 F5 preconditioning promoted proliferation and viability of H9-hNSCs 206
4.4.3 F5 preconditioning promoted astrocyte and neuronal differentiation of H9-hNSCs in the absence of growth factors..... 207
4.4.4 *HPRT1* and *RPL13A* as the best reference genes for control and F5-preconditioned H9-hNSCs..... 208
4.4.5 Upregulation of neuroprotective and paracrine effects following F5 preconditioning 209
4.5 Conclusion 216

CHAPTER 5 : THERAPEUTIC APPLICATIONS OF PRECONDITIONED H9-HNSCs ON *IN VITRO* ISCHEMIC STROKE (IVIS) MODEL 217
5.1 Introduction 217
5.1.1 Aims of work..... 218
5.1.2 Overview of this chapter 219
5.2 Methods..... 220
5.2.1 Developing an *in vitro* ischemic stroke (IVIS) model 220
5.2.1(a) Differentiation of SH-SY5Y cells..... 220
5.2.1(b) Morphological and ICC analyses 222

5.2.1(c) Oxygen-glucose deprivation/reperfusion (OGD/R)..... 222
5.2.1(d) Assessment of OGD/R-induced caspase 3 (CASP3) activation..... 223
5.2.2 Assessment of migration and homing capacities of hypoxic- and F5-preconditioned H9-hNSCs..... 223
5.3 Results..... 225
5.3.1 Development of *in vitro* model of neuronal cells..... 225
5.3.2 Development of IVIS model..... 227
5.3.3 Migration and homing potentials of hypoxic-preconditioned H9-hNSCs..... 231
5.3.4 Migration and homing potentials of F5-preconditioned H9-hNSCs..... 234
5.3.5 Comparison of migration and homing potentials between hypoxic- and F5-preconditioned H9-hNSCs..... 237
5.4 Discussion..... 239
5.4.1 ATRA-BDNF differentiated SH-SY5Y cells resembled *in vitro* model of human neuronal cells..... 239
5.4.2 IVIS model resembled OGD/R-induced neuronal injury..... 239
5.4.3 Hypoxic and F5 preconditioning enhanced migration and homing abilities of H9-hNSCs..... 241
5.4.4 F5 preconditioning provided a promising transplantation efficacy of H9-hNSCs..... 242
5.5 Conclusion..... 244

CHAPTER 6 : GENERAL DISCUSSION..... 245

6.1 Hypoxic preconditioning enhanced the therapeutic potentials of H9-hNSCs for ischemic stroke 245
6.2 F5 preconditioning enhanced the therapeutic potentials of H9-hNSCs for ischemic stroke 246
6.3 F5 preconditioning provided a promising efficacy of human NSC-based therapy for ischemic stroke 247

FUTURE STUDIES 249
CHAPTER 7 : CONCLUSION 250
REFERENCES 252
APPENDICES
Appendix A : Protocol for sterilization and aseptic techniques
Appendix B : Gradient PCR amplification of reference genes
Appendix C : Gradient PCR amplification of target genes
Appendix D : Voucher specimen of *O. indicum* for this study
Appendix E : Determination of optimal percentage of DMSO for H9-hNSCs
Appendix F : List of publications
Appendix G : List of posters and oral presentations

LIST OF TABLES

Page

Table 2.1 List of general instruments used in this study 50

Table 2.2 List of consumables used in this study 52

Table 2.3 List of chemicals and reagents used in this study 53

Table 2.4 List of antibodies used in this study 56

Table 2.5 List of primers used in this study 57

Table 2.6 List of software used in this study 59

Table 2.7 Absorption and emission spectra of fluorochrome used in this study 94

Table 3.1 The amplification efficiency and R^2 obtained from standard curves for each candidate reference gene used in the study 132

Table 3.2 NormFinder analysis for best candidate reference genes between normoxic- and hypoxic-preconditioned H9-hNSCs 139

Table 3.3 BestKeeper analysis of the candidate reference genes 142

Table 3.4 Ranking of candidate reference genes based on BestKeeper analysis 143

Table 3.5 Comprehensive ranking of the 10 candidate reference genes based on geometric mean of geNorm, NormFinder and BestKeeper ranking 145

Table 3.6 The amplification efficiency and R^2 obtained from standard curves for each target gene used in the study 150

Table 4.1 The yield of the methanol fractions obtained from *O. indicum*'s leaves 171

Table 4.2 Baicalein content from the crude extract and F5 178

Table 4.3 NormFinder analysis for best candidate reference genes between control and F5-preconditioned H9-hNSCs 198
Table 4.4 BestKeeper analysis of the candidate reference genes 200
Table 4.5 Ranking of candidate reference genes based on BestKeeper analysis 201
Table 4.6 Comprehensive ranking of the 10 candidate reference genes based on geometric mean of geNorm, NormFinder and BestKeeper ranking 203

LIST OF FIGURES

Page

Figure 1.1 A diagram illustrating (A) ischemic stroke and (B) hemorrhagic stroke 2

Figure 1.2 An overview of energy metabolism in the brain under (A) physiological conditions and (B) after ischemic stroke 4

Figure 1.3 An overview of cellular ion homeostasis under (A) physiological conditions and (B) after ischemic stroke 7

Figure 1.4 Glutamate homeostasis of presynaptic and postsynaptic neurons under (A) physiological conditions and (B) after ischemic stroke onset..... 9

Figure 1.5 Schematic illustration of free radical production and scavenging under (A) physiological conditions and (B) after ischemic stroke as indicated in red..... 12

Figure 1.6 Coronal section of human adult brain. 16

Figure 1.7 Representative images of *O. indicum.*..... 21

Figure 1.8 Preconditioning-induced neuroprotective signaling.. 23

Figure 1.9 Schema illustrating (A) HIF-1α domain structure, (B) PHD2 and (C) FIH-1 regulated HIF-1α degradation under normoxic conditions 24

Figure 1.10 Schematic illustration of HIF-1α stabilization under hypoxic conditions 26

Figure 1.11 Schematic illustration of (A) Notch 1 domain structure and (B) canonical and non-canonical Notch 1 signaling..... 28

Figure 1.12 Schematic representation of (A) *VEGFA* mRNA and (B) VEGFA signaling pathway 31
Figure 1.13 Schematic diagram illustrating (A) domain structure of ANGPT1 and (B) downstream signal transduction of ANGPT1-induced angiogenic effects 34
Figure 1.14 Schematic representation of (A) Nrf2 domains and (B) Nrf2 signaling upon stressed conditions 37
Figure 1.15 Schematic representation of (A) SOD1 structure and (B) disproportion of O_2•- by SOD1 40
Figure 1.16 Flowchart of the study overview 48
Figure 2.1 Fractionation of crude extract was performed using HP20 resin 98
Figure 3.1 Flowchart of the chapter overview 105
Figure 3.2 Representative phase-contrast images of H9-hNSCs preconditioned under normoxic (left panel) and hypoxic (right panel) settings for 6, 12, 24, 48, 72 and 96 h (n=3) 111
Figure 3.3 Percentage of viable H9-hNSCs after normoxic and hypoxic preconditioning for 6, 12, 24, 48, 72 and 96 h 112
Figure 3.4 Representative immunoblot of HIF-1α (upper panel) and β-actin (lower panel) protein expression (n=3) 114
Figure 3.5 HIF-1α expression in H9-hNSCs for 0, 6, 12, 24, 48, 72 and 96 h of hypoxia 115
Figure 3.6 Representative immunoblot of nestin (upper panel) and β-actin (lower panel) protein expression (n=3) 116
Figure 3.7 Nestin expression in H9-hNSCs for 0, 6, 12, 24, 48, 72 and 96 h of hypoxia 117

Figure 3.8 Representative image of normoxic- and hypoxic-preconditioned H9-hNSCs before (upper panel) and after (lower panel) astrocyte differentiation (n=3) 119

Figure 3.9 Representative immunofluorescence images of normoxic- and hypoxic-preconditioned H9-hNSCs before (upper panels) and after (lower panels) astrocyte differentiation (n=3) 120

Figure 3.10 The effects of hypoxic preconditioning on astrocyte differentiation potential of H9-hNSCs were deduced by quantitation of astrocytes 121

Figure 3.11 Representative images of normoxic- and hypoxic-preconditioned H9-hNSCs before (upper panel) and after (lower panel) neuronal differentiation (n=3) 123

Figure 3.12 Representative immunofluorescence images of normoxic- and hypoxic-preconditioned H9-hNSCs before (upper panels) and after (lower panels) neuronal differentiation (n=3) 124

Figure 3.13 The effects of hypoxic preconditioning on neuronal differentiation potential of H9-hNSCs were deduced by quantitation of neurons 125

Figure 3.14 'Bleach gel' electrophoresis of total RNA isolated from normoxic- and hypoxic-preconditioned H9-hNSCs (n=3) 127

Figure 3.15 Determination of qPCR amplification specificity for reference genes by melt curve analysis 129

Figure 3.16 Representative image of agarose gel (3%) electrophoresis showing amplification of a specific qPCR product of the expected size for each reference gene (n=3) 130

Figure 3.17 Standard curves for qPCR amplification efficiency calculation. 131

Figure 3.18 The expression levels (C_T value) of candidate reference genes in normoxic- and hypoxic-preconditioned H9-hNSCs 134

Figure 3.19 geNorm analysis of the candidate reference genes based on average expression stability value, plotted from the least stable (left) to the most stable (right). 136

Figure 3.20 Determination of the optimal number of reference genes based on geNorm analysis 137

Figure 3.21 Determination of qPCR amplification specificity of target genes by melt curve analysis. 147

Figure 3.22 Representative image of agarose gel (3%) electrophoresis showing amplification of a specific qPCR product of the expected size for each target gene (n=3) 148

Figure 3.23 Standard curves for qPCR amplification efficiency calculation 149

Figure 3.24 Upregulation of (A) *HIF-1α*, (B) *Notch 1*, (C) *nestin*, (D) *TUBB3*, (E) *VEGFA*, (F) *ANGPT1*, (G) *Nrf2* and (H) *SOD1* following hypoxic preconditioning 152

Figure 3.25 Hypoxic preconditioning modulated transcript levels of *HIF-1α*, *Notch 1*, *nestin*, *TUBB3*, *VEGFA*, *ANGPT1*, *Nrf2* and *SOD1*..... 158

Figure 4.1 Flowchart of the chapter overview 165

Figure 4.2 TLC separation of baicalein standard (B), crude extract (CE) and methanol fractions (F1-F5) 172

Figure 4.3 Absorbance spectra of baicalein standard (10 μg/mL) within 250 and 800 nm 174

Figure 4.4 Chromatogram of baicalein standard (upper panel) and crude extract (lower panel) of *O. indicum*..... 175

Figure 4.5 Chromatogram of (A) F1, (B) F2, (C) F3, (D) F4 and (E) F5 of *O. indicum* 176

Figure 4.6 Calibration curve of baicalein standard was plotted using peak height (y-axis) against weight (μg). 177

Figure 4.7 Representative phase-contrast images showed the effects of F5 on H9-hNSCs at different concentrations and durations (n=3)..... 180

Figure 4.8 Percentage of viable H9-hNSCs after F5 preconditioning for 24, 48 and 72 h 181

Figure 4.9 Representative images of control and F5-preconditioned H9-hNSCs before (upper panel) and after (lower panel) astrocytic differentiation (n=3)..... 183

Figure 4.10 Representative immunofluorescence images of control and F5-preconditioned H9-hNSCs before (upper panels) and after (lower panels) astrocyte differentiation (n=3)..... 184

Figure 4.11 The effects of F5 preconditioning on astrocyte differentiation potential of H9-hNSCs were deduced by quantitation of astrocytes 185

Figure 4.12 Representative images of control and F5-preconditioned H9-hNSCs before (upper panel) and after (lower panel) neuronal differentiation (n=3) 187

Figure 4.13 Representative immunofluorescence images of control and F5-preconditioned H9-hNSCs before (upper panels) and after (lower panels) neuronal differentiation (n=3) 188

Figure 4.14 The effects of F5 preconditioning on neuronal differentiation potential of H9-hNSCs were deduced by quantitation of neurons ... 189

Figure 4.15 'Bleach gel' electrophoresis of total RNA isolated from control and F5-preconditioned H9-hNSCs (n=3) 191

Figure 4.16 The expression levels (C_T value) of candidate reference genes in control and F5-preconditioned H9-hNSCs 193

Figure 4.17 geNorm analysis of the candidate reference genes based on average expression stability value, plotted from the least stable (left) to the most stable (right) 195

Figure 4.18 Determination of the optimal number of reference genes based on geNorm analysis 196

Figure 4.19 Upregulation of (A) *HIF-1α*, (B) *Notch 1*, (C) *nestin*, (D) *TUBB3*, (E) *VEGFA*, (F) *ANGPT1*, (G) *Nrf2* and (H) *SOD1* following F5 preconditioning 205

Figure 4.20 F5 preconditioning modulated transcript levels of *HIF-1α*, *Notch 1*, *nestin*, *TUBB3*, *VEGFA*, *ANGPT1*, *Nrf2* and *SOD1*. 211

Figure 4.21 Schematic illustration of auto-oxidation of baicalein by molecular oxygen 214

Figure 5.1 Flowchart of the chapter overview 219

Figure 5.2 A schematic timeline of the experimental design for the differentiation of SH-SY5Y cells using sequential treatment with ATRA and BDNF 221

Figure 5.3 Assessment of migration potential of (A) normoxic-, (B) hypoxic-, (C) control (0.1% DMSO) and (D) F5-preconditioned

H9-hNSCs towards IVIS model using fibronectin coated SPLScar™ block cell culture slide 224

Figure 5.4 Representative phase-contrast images for development of *in vitro* neuronal cells model (n=3) 226

Figure 5.5 Representative immunofluorescence images of SH-SY5Y cells before (upper panel) and after (lower panel) ATRA-BDNF differentiation (n=3) 228

Figure 5.6 Representative phase-contrast images for development of IVIS model (n=3) 229

Figure 5.7 Representative immunofluorescence images of differentiated SH-SY5Y cells before (upper panel) and after (lower panel) OGD/R (n=3) 230

Figure 5.8 Bright-field live imaging at 0, 24, 48 and 72 h on migration assessment of normoxic- (left panel) and hypoxic-preconditioned (right panel) H9-hNSCs towards IVIS model (n=3) 232

Figure 5.9 Representative immunofluorescence images of migration assessment of normoxic- (left panel) and hypoxic-preconditioned (right panel) H9-hNSCs towards IVIS model after 72 h (n=3) 233

Figure 5.10 Bright-field live imaging demonstrated migration of control (left panel) and F5-preconditioned (right panel) H9-hNSCs towards IVIS model at 0, 24, 48 and 72 h (n=3) 235

Figure 5.11 Representative immunofluorescence images showed migration potential of control (left panel) and F5-preconditioned (right panel) H9-hNSCs towards IVIS model after 72 h (n=3)..... 236

Figure 5.12 Migration potential of hypoxic- and F5-preconditioned H9-hNSCs towards IVIS model after 72 h..... 238

LIST OF SYMBOLS, ABBREVIATIONS AND ACRONYMNS

ACTB	β-actin
ARE	Antioxidant response element
ATP	Adenosine triphosphate
ATRA	All-*trans* retinoic acid
ANGPT1	Angiopoietin-1
BDNF	Brain-derived neurotrophic factor
bFGF	Basic fibroblast growth factor
BLAST	Basic local alignment search tool
BSA	Bovine serum albumin
CBP	CREB-binding protein
cDNA	Complementary deoxyribonucleic acid
CSL	CBF1/Su(H)/Lag-1
CV	Coefficient of variance
DMSO	Dimethyl sulfoxide
DNase	Deoxyribonuclease
EDTA	Ethylenediaminetetraacetic acid
EGF	Epidermal growth factor
EtBr	Ethidium bromide
elF4A	Eukaryotic initiation factor 4A
ERK	Extracellular signal-recegulated kinase
ETC	Electron transport chain
$FADH_2$	Flavin adenine dinucleotides
FBS	Fetal bovine serum
FIH-1	Factor inhibiting HIF-1

GAPDH	Glyceraldehyde-3-phosphate dehydrogenase
GFAP	Glial fibrillary acidic protein
GPx	Glutathione peroxidase
HIF	Hypoxia-inducible factor
HPLC	High performance liquid chromatography
HPRT1	Hypoxanthine phosphoribosyl transferase 1
HRE	Hypoxia response element
HRP	Horseradish peroxidase
ICC	Immunocytochemistry
IVIS	*In vitro* ischemic stroke
IPO8	Importin 8
KEAP 1	Kelch-like ECH-associated protein 1
MAPK	Mitogen-activated protein kinase
MPTP	Mitochondrial permeability transition pore
NADH	Nicotinamide adenine dinucleotide
NADPH	Nicotinamide adenine dinucleotide phosphate
NICD	Notch 1 intracellular domain
Notch 1	Neurogenic locus notch homolog protein 1
Nrf2	Nuclear factor erythroid 2-related factor 2
NSC	Neural stem cell
OD	Optical density
OG	Oxoglutarate
OGD/R	Oxygen-glucose deprivation/reperfusion
O. indicum	*Oroxylum indicum*
OXPHOS	Oxidative phosphorylation

PBS	Phosphate-buffered saline
PFA	Paraformaldehyde
PHD2	Prolyl hydroxylase 2
PKC	Protein kinase C
PPIA	Peptidyl-prolyl isomerase A
PVDF	Polyvinylidene fluoride
qPCR	Quantitative real-time polymerase chain reaction
RAM	RBPJ-associated molecule
RNA	Ribonucleic acid
ROS	Reactive oxygen species
RPL13A	Ribosomal protein L13A
RPLP1	60S ribosomal protein large P1
r-tPA	Recombinant tissue plasminogen activator
TUBB3	Tubulin β 3 class III
SD	Standard deviation
SDS	Sodium dodecyl sulphate
SEM	Standard error of means
SGZ	Subgranular zone
SOD	Superoxide dismutase
SVZ	Subventricular zone
TBP	TATA box binding protein
TCA	Tricarboxylic acid
TEMED	Tetramethylenediamine
TLC	Thin layer chromatography
UV	Ultraviolet

VDAC	Voltage-dependent anion-selective channel
VEGFA	Vascular endothelial growth factor A
XDH	Xanthine dehydrogenase
XO	Xanthine oxidase
YWHAZ	Tyrosine 3-monooxygenase/tryptophan 5-monooxygenase activation protein, zeta polypeptide
α	Alpha
NH_2	Amine
et al.	And others
β	Beta
bp	Base pair
Ca	Calcium
Cu	Copper
CO_2	Carbon dioxide
COOH	Carboxyl
coQ	Coenzyme Q
Cyt c	Cytochrome c
Da	Dalton
^{o}C	Degree celcius
Δ	Delta
E	Efficiency of primer
Fe	Iron
γ	Gamma
g	Gram
h	Hour

HCl	Hydrochloric acid
H_2O_2	Hydrogen peroxide
$^{\bullet}OH$	Hydroxyl radical
IgG	Immunoglobulin G
κ	Kappa
k	Kilo
L	Litre
µ	Micro
m	Milli
min	Minute
M	Molar
n	Nano
N_2	Nitrogen
N	Normality
O_2	Oxygen
pH	Potential of hydrogen
K	Potassium
Psi	Pound of force per square inch of area
p	Probability
Pro	Proline
Akt	Protein kinase B
H^+	Proton
®	Registered
$^1O_2$	Singlet oxygen
$O_2^{\bullet-}$	Superoxide anion

s	Second
Na	Sodium
NaOH	Sodium hydroxide
MTT	Tetrazolium
C_T	Threshold cycle
™	Trademark
Tie-2	Tyrosine kinase-2
vs	Versus
V	Volt
v/v	Volume/volume
w/v	Weight/volume
X g	Times gravity
Zn	Zinc

POTENSI TERAPEUTIK SEL STEM NEURAL MANUSIA ARUHAN SECARA HIPOKSI DAN FRAKSI KAYA DENGAN *BAICALEIN* UNTUK MODEL STROK ISKEMIA *IN VITRO*

ABSTRAK

Strok iskemia merupakan punca utama kematian di Malaysia selepas penyakit jantung dan barah. Kaedah rawatan biasa tidak mampu memulih dan menjana semula tisu otak pesakit yang mati. Sel stem neural dewasa dalam otak juga tidak mampu memulih tisu tersebut berikutan kadar penjanaan sel neuron yang terhad gagal membentuk jaringan saraf. Oleh yang demikian, pesakit strok berisiko tinggi untuk serangan semula. Kaedah alternatif berasaskan terapeutik adalah penting untuk meningkatkan pemulihan strok. Mutakhir ini, transplantasi sel stem neural manusia telah menjadi pendekatan terbaik untuk rawatan penyakit neurodegeneratif termasuk strok. Namun demikian, potensi transplantasi sel stem neural adalah terhad kerana kegagalan sel tersebut untuk bertahan dalam kawasan iskemia. Kajian ini bertujuan untuk mengatasi kelemahan tersebut dengan meningkatkan potensi terapeutik sel stem neural melalui aruhan secara hipoksi dan fraksi kaya dengan *baicalein* (F5). Hipoksia paras fisiologi (2% O_2) selama 24 jam meningkatkan proliferasi, ketahanan dan keupayaan membeza kepada pelbagai jenis sel neural matang. Gen rujukan protein ribosom sub unit besar P1 (*RPLP1*) dan protein ribosom sub unit besar L13A (*RPL13A*) adalah sesuai untuk normalisasi data tindak balas berantai polimerase kuantitatif (qPCR) sel stem neural aruhan secara normoksi dan hipoksi. Aruhan hipoksia mengaktifkan isyarat perlindugan dalam sel melalui transkripsi faktor pendorongan hipoksia-1 alfa (*HIF-1α*), faktor pertumbuhan endotelial vaskular A (*VEGFA*), angiopoietin 1 (*ANGPT1*), protein homolog 1 notch lokus neurogenik

(*Notch 1*), faktor berkait 2-eritroid faktor nukleus 2 (*Nrf2*) and dismutasi natrium (*SOD1*). F5 dipilih sebagai agen aruhan kerana mengandungi *baicalein* yang merupakan penstabil HIF-1α mimik aruhan hipoksi walaupun dalam keadaan normoksia. Sel stem neural diaruh dengan 1.56 μg/mL F5 selama 24 jam juga meningkatkan proliferasi, ketahanan dan potensi sel stem neural untuk menjana sel otak matang. Hipoksanthin fosforibosil transferas (*HPRT1*) dan *RPL13A* adalah gen rujukan paling stabil bagi sel stem neural kawalan (0.1% DMSO) dan aruhan secara F5. Seperti hipoksia, aruhan F5 mendorong kepada pengaktifan *HIF-1α*, *VEGFA*, *ANGPT1*, *Notch 1*, *Nrf2* and *SOD1*. Sel stem neural aruhan secara hipoksi dan F5 digunakan untuk merawat model strok iskemia *in vitro* (IVIS). Aruhan F5 menunjukkan kelebihan pertumbuhan lebih pantas menghampiri model IVIS berbanding aruhan hipoksia. Faktor pelindung berpontesi yang dirangsang oleh aruhan hipoksia mempunyai jangka hayat singkat dalam keadaan beroksigen. Aruhan F5 merangsang faktor perlindungan berpotensi yang stabil tanpa dipengaruhi oleh oksigen. Aruhan secara hipoksi dan F5 telah meningkatkan potensi terapeutik sel stem neural untuk terapeutik strok. Kajian ini menunjukkan bahawa sel stem neural diaruh F5 terbukti mempunyai potensi terapeutik yang tinggi, di samping sesuai digunakan secara klinikal untuk rawatan strok iskemia pada masa hadapan.

THERAPEUTIC POTENTIALS OF HYPOXIC- AND BAICALEIN-ENRICHED FRACTION-PRECONDITIONED HUMAN NEURAL STEM CELLS FOR *IN VITRO* ISCHEMIC STROKE MODEL

ABSTRACT

Ischemic stroke is the third leading cause of death in Malaysia, closely after heart disease and cancer. Standard treatments for stroke are not totally efficient to repair and regenerate the damaged brain tissue and there are possibilities for the recurrence. Replacement by endogenous adult neural stem cells (NSCs) during ischemic stroke was insufficient to repair injury site due to low neuronal turnover that could integrate into functional neuron network. Therefore, it is imperative to develop alternative therapeutic strategies to improve stroke recovery. Recently, human NSC grafting has emerged as encouraging approach for treating stroke. Nonetheless, the therapeutic potential of NSC-based treatment is limited, mainly due to a large number of implanted cells died after grafting into the injury site. To circumvent this problem, this study aimed to enhance therapeutic potentials of human NSCs prior to transplantation through hypoxic and baicalein-enriched fraction (F5) preconditioning. Hypoxic preconditioning under 2% O_2 for 24 h enhanced NSC self-renewal, survival and multipotency. 60S ribosomal protein large P1 (*RPLP1*) and ribosomal protein L13A (*RPL13A*) were the most reliable reference genes for qPCR normalization of normoxic- and hypoxic-preconditioned NSCs. Hypoxic preconditioning induced innate neuroprotective signaling through transcriptional activation of hypoxia-inducible factor-1 alpha (*HIF-1α*), vascular endothelial growth factor A (*VEGFA*), angiopoietin 1 (*ANGPT1*), neurogenic locus notch homolog protein 1 (*Notch 1*), nuclear factor erythroid 2-related factor 2 (*Nrf2*) and sodium

dismutase 1 (*SOD1*). Based on the HIF-1α stabilization potential of baicalein at ambient conditions, F5 was postulated to trigger effects mimic hypoxic preconditioning under normoxia. Interestingly, preconditioning with 1.56 μg/mL of F5 for 24 h increased NSC proliferation, viability and lineage specific differentiation. Hypoxanthine phosphoribosyl transferase 1 (*HPRT1*) and *RPL13A* were the most stably expressed reference genes for qPCR normalization of control (0.1% DMSO) and F5-preconditioned NSCs. Moreover, F5 preconditioning stimulated hypoxia-mimetic signaling intrinsically via *HIF-1α*, *VEGFA*, *ANGPT1*, *Notch 1*, *Nrf2* and *SOD1* upregulation. Both hypoxic- and F5-preconditioned NSCs were applied to *in vitro* ischemic stroke (IVIS) model on wound-healing based culture slide for 72 h of live imaging. F5-preconditioned NSCs accelerated migration and homing towards IVIS model over an experimental period of 72 h compared to hypoxic-preconditioned NSCs. The neuroprotective factors induced by hypoxic preconditioning are postulated to degrade rapidly when exposed to oxygen. Contrarily, F5-preconditioned NSCs attained intrinsic neuroprotective mechanisms without compromising their stability under normoxia. In conclusion, both the hypoxic and F5 preconditioning had successfully enhanced therapeutic potentials of NSCs for ischemic stroke. F5-preconditioned NSCs with enhanced therapeutic efficacy was more likely to be applicable in clinical setting and thus could be a promising therapeutic tool for ischemic stroke in the future.

CHAPTER 1

INTRODUCTION

1.1 Stroke

Stroke, the nation's third leading cause of death, leading to severe and long-term functional disability (Loo and Gan, 2012; Cheah *et al.*, 2016). In Malaysia, most patients had ischemic stroke rather than hemorrhagic stroke (Jaya *et al.*, 2002). Ischemic stroke is characterized by thrombotic or embolic occlusion of cerebral artery, thereby restricts oxygen, nutrients and glucose supplies to an area of the brain (Figure 1.1A). In contrary, hemorrhagic stroke is characterized by rupture of a blood vessel on or within the brain, subsequently causing severe bleeding into brain parenchyma (Figure 1.1B). According to National Health and Morbidity Survey (NHMS), the prevalence of stroke among Malaysians increased between 2006 and 2011 (Cheah *et al.*, 2016). As a result, stroke causes an economic burden on health-care budgets and the whole nation economic development.

A

B

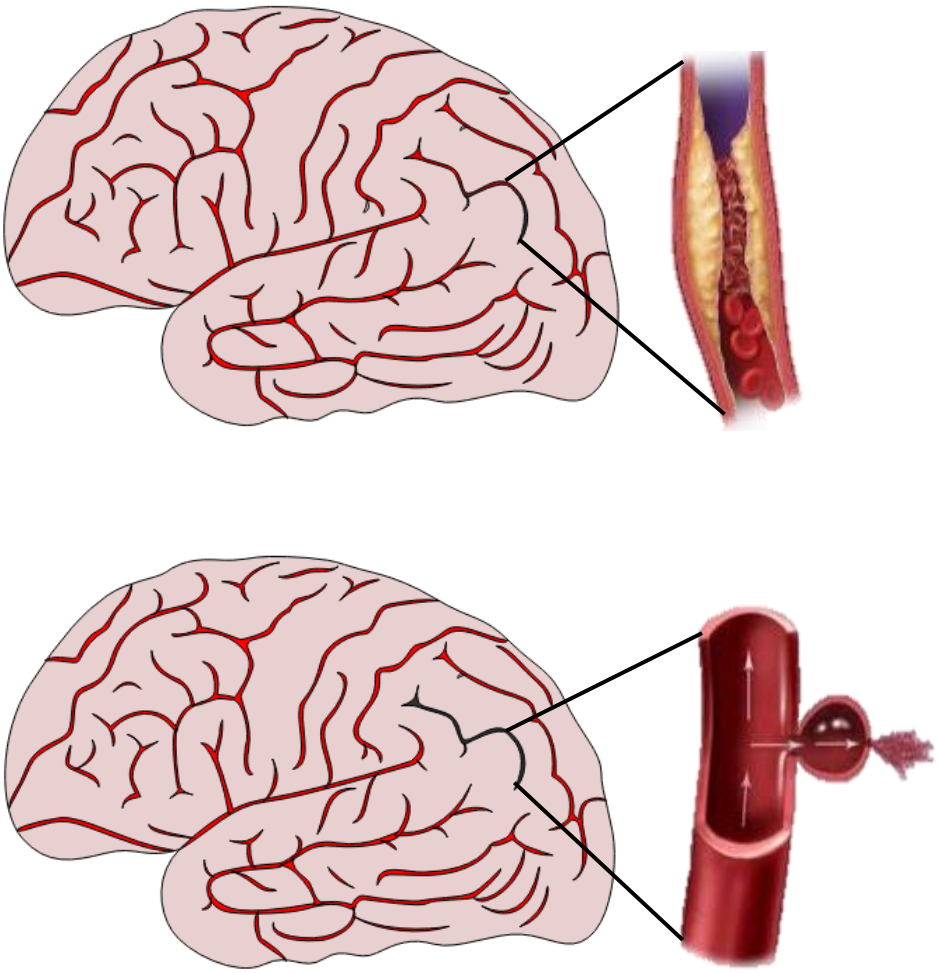

Figure 1.1 A diagram illustrating (A) ischemic stroke and (B) hemorrhagic stroke. Ischemic stroke occurs when a clot blocks blood flow to an area of the brain. Hemorrhagic stroke occurs when blood vessels rupture causing blood leakage into cerebral parenchyma. Figure is generated using Edraw Max software and Microsoft PowerPoint.

1.1.1 Pathophysiologic cascades in ischemic stroke

Ischemic stroke initiates a cascade of pathophysiologic cellular and molecular mechanisms such as energy failure, ionic imbalance, glutamate excitotoxicity, inflammation and free radical overload, resulting in irreversible brain damage (Deb *et al.*, 2010).

1.1.1(a) Energy failure

Glucose is the primary energy source for the brain (Mergenthaler *et al.*, 2013). Nonetheless, the brain does not store glucose and hence requires a constant supply of glucose (Berg *et al.*, 2002). Due to high energy consumption, abundance mitochondria are present in neurons (Misgeld and Schwarz, 2017). Under physiological conditions, neurons depend mainly on mitochondrial oxidative phosphorylation (OXPHOS) as the main source of adenosine triphosphate (ATP) (Figure 1.2A) (Zheng *et al.*, 2016). This is because OXPHOS generates energy in the form of 36 molecules of ATP for each molecule of glucose (Valvona *et al*., 2015).

Glucose is metabolized to pyruvate through glycolysis (Valvona *et al*., 2015). This process also generates ATP and nicotinamide adenine dinucleotides (NADH). Pyruvate enters mitochondria and gets oxidized into acetyl-coA, CO_2 and NADH. Acetyl-coA is subsequently oxidized in tricarboxylic acid cycle (TCA). TCA cycle provide NADH and flavin adenine dinucleotides ($FADH_2$) which carry the high-energy electron for OXPHOS at the inner mitochondrial membrane (Lodish *et al.*, 2000). The inner mitochondrial membrane comprises complex I, II, III, IV and V. During OXPHOS, electron transport chain (ETC) passes electrons released from reduced form of NADH and $FADH_2$ to complex I and II, respectively

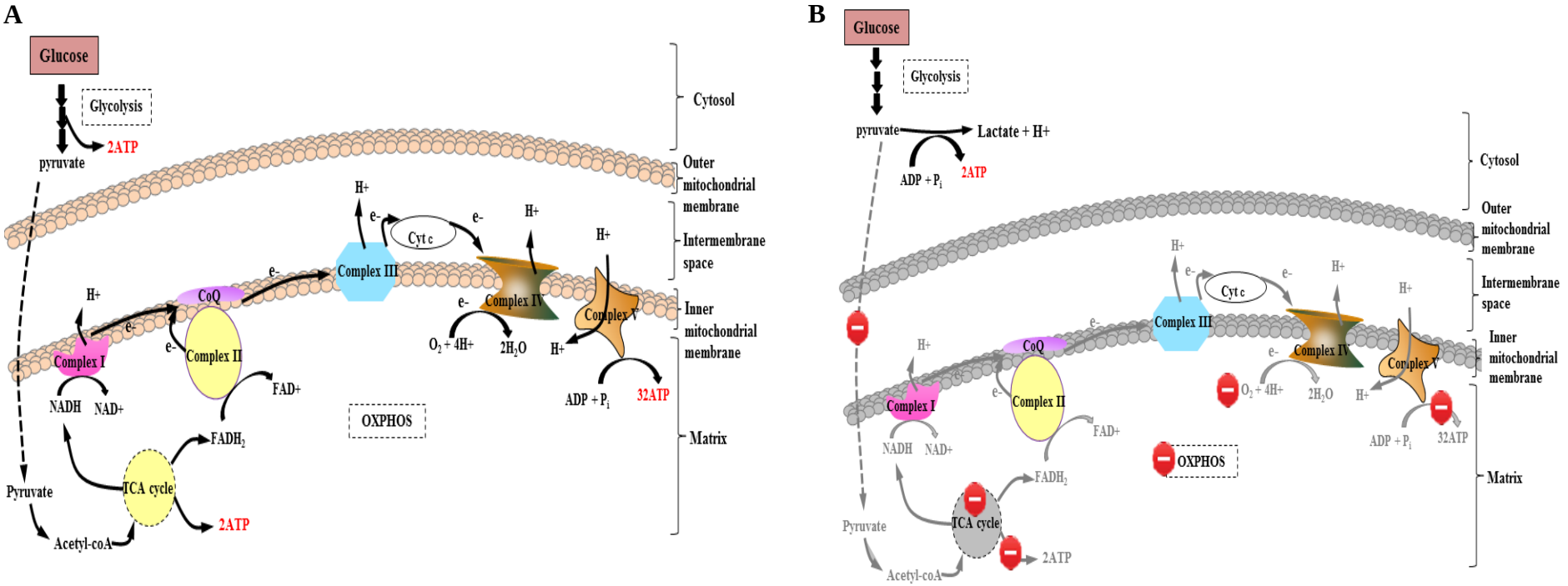

Figure 1.2 An overview of energy metabolism in the brain under (A) physiological conditions and (B) after ischemic stroke. (A) Glucose is converted into pyruvate via glycolysis in the cytosol. Pyruvate is transported into the mitochondria and oxidized to form acetyl-coA. Acetyl-coA is subsequently oxidized via TCA cycle, releasing NADH, $FADH_2$ and ATP. The electrons transfer from reduced NADH and $FADH_2$ to oxygen in a series of redox reactions. These reactions released free energy in a form of H^+ gradient across the inner mitochondrial membrane, resulting in ATP synthesis via chemiosmosis. (B) Due to disrupted blood flow, oxygen and glucose levels eventually drop too low for mitochondrial OXPHOS, causing oxidative stress on mitochondria. To compensate the energy supply, glucose is converted into pyruvate via anaerobic glycolysis to meet the metabolic demands. Pyruvate is then converted into the lactate and H^+. Nevertheless, these reactions generate only 2 molecules of ATP for each molecule of glucose. Ultimately, anaerobic glycolysis fails to compensate the high energy demand of brain cells, leading to energy exhaustion. High accumulation of lactate and H^+ may also lead to acidosis. Figure is generated using Cell Illustrator 5 and Microsoft PowerPoint.

(Lodish *et al.*, 2000). Electrons are then transferred from both complexes to coenzyme Q (coQ). Coenzyme Q transports electrons to complex III and then to cytochrome c (Cyt c). The ETC ends at complex IV where electrons reduce oxygen in the presence of proton (H^+) to water. The electrons transfer across complex I, III and IV is also coupled to H^+ transfer, hence, generating a H^+ gradient across the inner mitochondrial membrane (Lodish *et al.*, 2000). Complex V uses the free energy released from H^+ gradient along with ATP synthase to convert adenosine diphosphate (ADP) and inorganic phosphate (P_i) into ATP.

In brain, neurons constantly demand for high glucose to perform basic cellular processes such as protein synthesis and energy production (Bédanger *et al.*, 2011; Niven, 2016). Complete loss of blood flow to the brain for only 5 min is deadly to neurons (Lipton, 1999). During ischemic stroke, interruption of blood flow attributes to oxygen and glucose deprivation (OGD). Upon OGD insults, continuous consumption of oxygen and glucose diminish their availability for mitochondrial OXPHOS and ATP generation (Figure 1.2B). Following that, the glucose metabolism switches from aerobic to anaerobic glycolysis for ATP production until glucose is completely depleted (Solaini *et al.*, 2010). Nevertheless, the efficiency of ATP production by anaerobic glycolysis is much lower compared to mitochondrial OXPHOS in which only 2 molecules of ATP produced for each molecule of glucose under anaerobic conditions. Unfortunately, consumption exceeds production and drives energy failure in the brain. In addition, anaerobic glycolysis also produces H^+ and lactate, lowering the pH and causing rapid intracellular acidosis (Solaini *et al.*, 2010).

1.1.1(b) Ionic imbalance

Under physiological conditions, the potassium ion (K^+) level has higher concentrations intracellular than extracellular (Figure 1.3A) (Cheng *et al.*, 2013). However, the intracellular levels of sodium ion (Na^+) and calcium ion (Ca^{2+}) are lower than extracellular (Cheng *et al.*, 2013). Following rapid ATP deficit, activity of ATP-dependent transport systems such as Na^+/K^+-ATPase, K^+/Ca^{2+}-ATPase and Ca^{2+}-ATPase pumps are reduced (Figure 1.3B). As consequence, the K^+ channels open and permit K^+ to move outward, leading to accumulation of extracellular K^+ levels. Hence, the cells are hyperpolarize and change the gradient concentrations of Na^+ and K^+ across the plasma membrane (Reading and Isbir, 1980). The Na^+ channels close and retain Na^+ intracellular, leading to accumulation of Na^+ in the cells and depolarization of the membrane potential. Hyperpolarized cells also activate voltage-gated calcium channels which lead to Ca^{2+} influx. Ca^{2+} is an intracellular messenger participating in many cellular processes, particularly in signal transduction pathways (Hofer and Lefkimmiatis, 2007). Overload of Ca^{2+} in the cell further contributes to collapse of membrane potential. Ionic imbalances also induce transient osmotic gradients in the brain as water influx towards area of high Na^+ levels, resulting in cell swelling and edema (Rungta *et al.*, 2015).

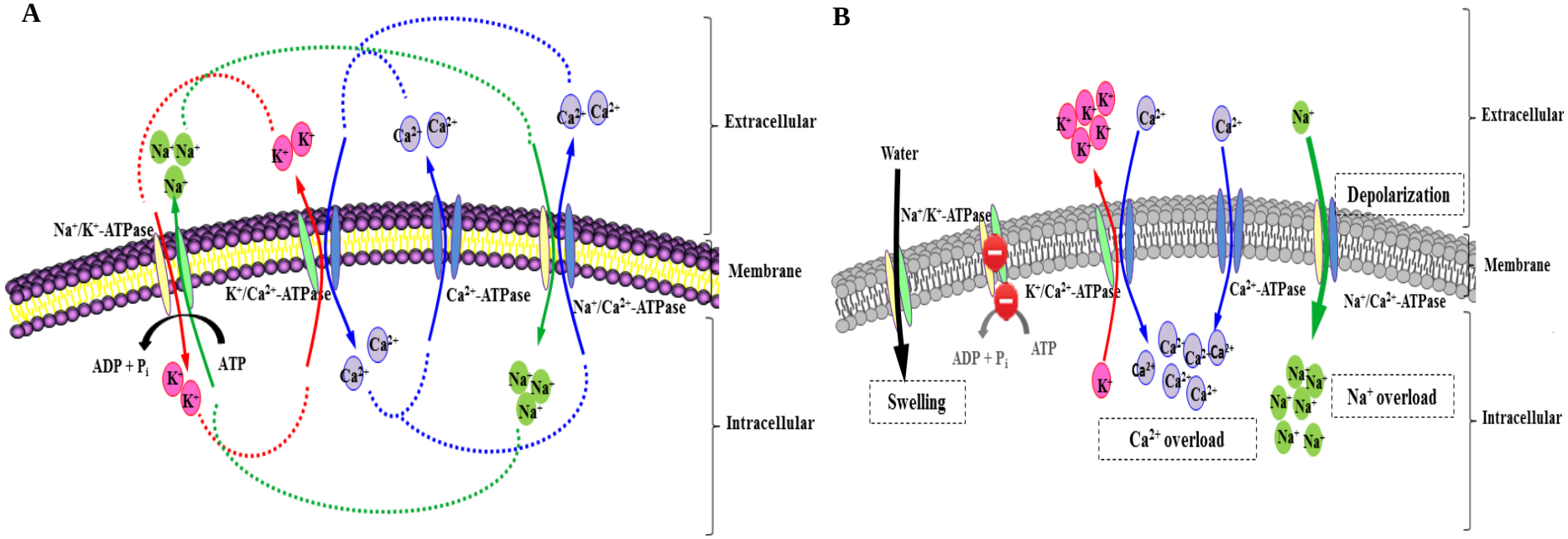

Figure 1.3 An overview of cellular ion homeostasis under (A) physiological conditions and (B) after ischemic stroke. (A) Under physiological conditions, Na^+/K^+-ATPase uses ATP to pump out 3 Na^+ and take in 2 K^+. The ionic balance is maintained by K^+/Ca^{2+}-ATPase which pumps out the K^+ and takes in Ca^{2+}. Na^+/Ca^{2+}-ATPase maintains the intracellular Ca^{2+} by pumping out Ca^{2+} and takes in Na^+. Hence, the K^+ level is higher intracellular whereas Na^+ and Ca^{2+} levels are lower intracellular. (B) Due to disrupted blood flow, oxygen and glucose levels eventually drops too low for energy metabolism, causing rapid declination of ATP. As a consequence, ATP-dependent transport systems such as Na^+/K^+-ATPase, K^+/Ca^{2+}-ATPase and Ca^{2+}-ATPase pumps fail to distribute respective ions across the membrane, leading to ionic imbalance. The effects of changes in ion concentration gradient promote depolarization of membrane potential and cell swelling. Figure is generated using Cell Illustrator 5 and Microsoft PowerPoint.

1.1.1(c) Glutamate excitotoxicity

Neurotransmitters are chemical messengers that enable excitatory or inhibitory neurotransmission to pass an electrical or chemical signal from a neuron to a target neuron across the synapse (Deutch, 2013). Glutamate is an amino acid-based excitatory neurotransmitter which constitutes for over 90% of the synapses in human brain (Hofmeijer and van Putten, 2012). It is a non-essential amino acid derived from reductive amination of a TCA cycle intermediate, α-ketoglutarate (Schousboe *et al.*, 2014). Alternatively, glutamate can be synthesized from hydrolysis of glutamine by phosphate activated glutaminase in presynaptic neuron or surrounding glial cells (Schousboe *et al.*, 2014). Under physiological conditions, glutamate is cleared from the synaptic cleft by Na^+-coupled glutamate transporters on the plasma membrane of presynaptic terminal and glial cells. In the presynaptic terminal, glutamate is stored in vesicles at the axon (Figure 1.4A). In glial cells, glutamate is converted to glutamine by glutamine synthase in the presence of ATP before being transported back to presynaptic terminal. The glutamine is then recycled for glutamate synthesis in the presynaptic terminal. However, under OGD conditions, lack of ATP production and impairment of Na^+/K^+-ATPase increase intracellular Na^+ and extracellular K^+, which facilitate release of glutamate from the synaptic vesicles into the synaptic cleft (Grewer *et al.*, 2008). Excess accumulation of extracellular glutamate over-activates the glutamate receptors. Following excitatory stimulation, massive extracellular Ca^{2+} enters the postsynaptic neuron through ionotropic glutamate receptors such as N-methyl-D-aspartate receptors (NMDARs), leading to phospholipases and proteases accumulation which perturbed the cellular integrity (Figure 1.4B). Ultimately, glutamate excitotoxicity triggers depolarization of postsynaptic neuron, leading to neuronal death (Grewer *et al.*, 2008).

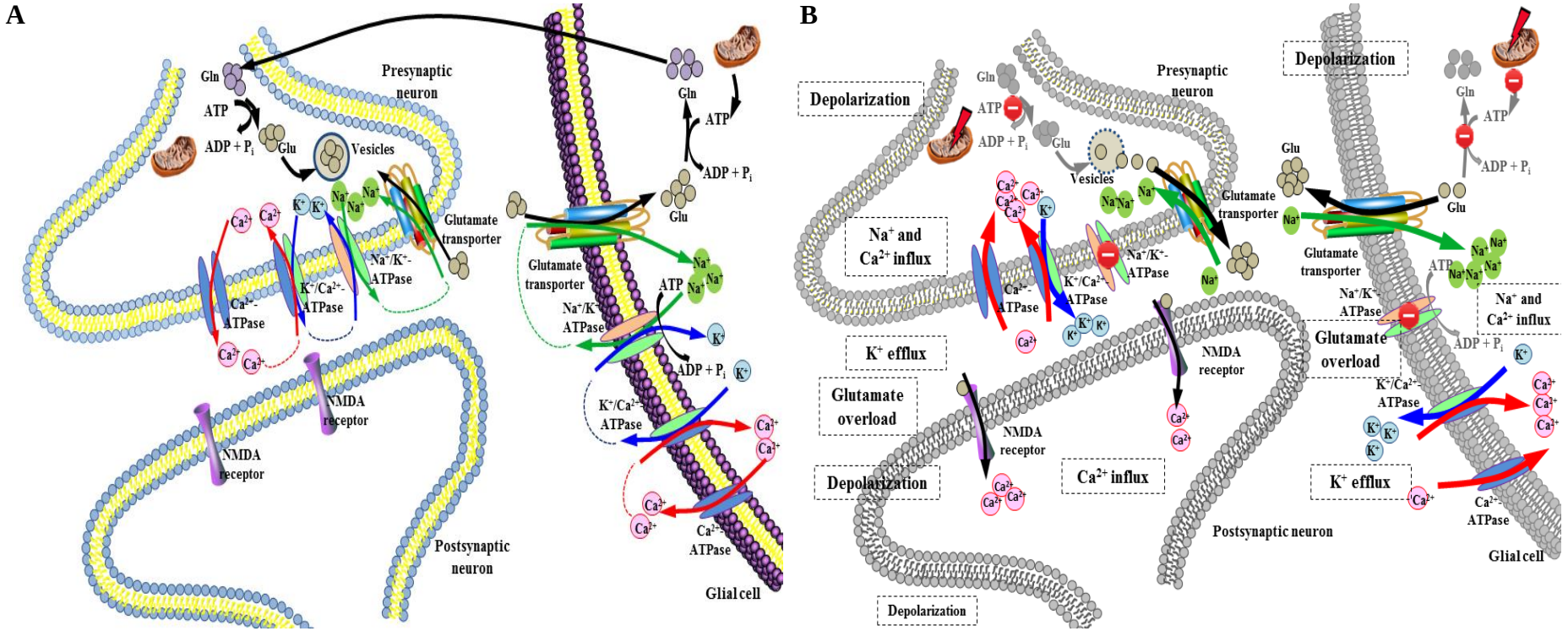

Figure 1.4 Glutamate homeostasis of presynaptic and postsynaptic neurons under (A) physiological conditions and (B) ischemic stroke onset. (A) Under basal condition, glutamate transporters remove glutamate (Glu) from extracellular space and stored in vesicles. In glial cells, glutamate is converted to glutamine (Gln) by glutamine synthase in the presence of ATP before being transported back to presynaptic terminal. The glutamine is then recycled for glutamate synthesis in the presynaptic terminal. The K^+ level is maintained at higher level intracellular. Na^+ and Ca^{2+} levels are maintained at lower levels intracellular. (B) Under pathological conditions, lack of ATP production and impairment of Na^+/K^+-ATPase increase intracellular Na^+ and Ca^{2+} whilst reducing intracellular K^+, which induce trafficking of glutamate transporters backwards causing glutamate excitotoxicity. Ultimately, depolarization of postsynaptic neuron led to neuronal death. Figure is generated using Cell Illustrator 5 and Microsoft PowerPoint.

1.1.1(d) Inflammation

The onset of ischemic stroke also initiates various inflammatory cascades by inflammatory cells such as leucocytes, endothelial cells, astrocytes and microglia to produce pro-inflammatory cytokines and adhesion molecules (Lambertsen *et al.*, 2012). Circulating leucocytes then migrate and accumulate in the infarcted lesion before secreting pro-inflammatory mediators which trigger additional injury on neighboring viable cells surrounding the lesion (Vexler *et al.*, 2006). Microglial cells are resident immune cells in the brain (Lull and Block, 2010). Activation of microglia leads to morphologic transformation into phagocytes, subsequently exerting macrophagic functions including phagocytosis, secretion of pro-inflammatory cytokines and generation of reactive oxygen species (ROS) (Lull and Block, 2010). Under pathological conditions, pro-inflammatory cytokines promote the infiltration of inflammatory cells from the circulation into the tissues (Dinarello, 2009). In addition, accumulation of pro-inflammatory cytokines also promotes inflammatory injury through glutamate-mediated excitotoxicity (Olmos and Lladó, 2014).

1.1.1(e) Free radical production

Normally, mitochondrial OXPHOS converts oxygen molecules into ATP and water. Occasionally, mitochondrial ETC may leak electrons directly to oxygen, resulting in free radical formation. Besides mitochondrial ETC, several cytosolic enzymes such as xanthine oxidase (XO) also contribute to free radical production (Görlach *et al.*, 2015). Free radicals are oxygen-derived oxidants known as ROS. ROS produced in mitochondrial OXPHOS include hydroxyl radical ($^{\bullet}OH$), superoxide anion ($O_2^{\bullet-}$), singlet oxygen ($^1O_2$) and hydrogen peroxide (H_2O_2)

(Halliwell and Gutteridge, 2015). As illustrated in Figure 1.5A, $O_2^{\bullet-}$ is released from complex I and II into the matrix during electron transport. In addition, complex III also generates $O_2^{\bullet-}$ within intermembrane space. The latter could be transported through outer mitochondrial membrane by voltage-dependent anion-selective channel (VDAC).

Under physiological conditions, ROS is maintained at low levels by intrinsic antioxidant systems such as catalases, superoxide dismutase (SOD) and glutathione peroxidase (GPx) (Figure 1.5A). In cytosol and intermembrane space of mitochondria, SOD1 converts $O_2^{\bullet-}$ into H_2O_2 and water. In mitochondrial matrix, SOD2 is responsible for the $O_2^{\bullet-}$ dismutation. The glutathione peroxidase enzyme (GPx) in the matrix and catalase enzyme in the cytosol catalyse reduction of H_2O_2 into water and oxygen.

Upon ischemia, impaired oxygen supply leads to ATP depletion. Due to ongoing cellular metabolism and ineffective rephosphorylation, ATP is degraded to hypoxanthine. Ca^{2+} influx also activates Ca^{2+}–dependent protease to oxidize xanthine dehydrogenase (XDH) to XO, $O_2^{\bullet-}$ and H_2O_2. However, XO is unable to convert hypoxanthine to xanthine in the absence of oxygen, leading to accumulation of hypoxanthine. H_2O_2 is partially reduced to highly damaging $^{\bullet}OH$. In addition, impaired oxygen supply causes heme proteins to release ferrous cation (Fe^{2+}). The Fe^{2+} reacts with H_2O_2 at higher affinity, giving rise to $^{\bullet}OH$ through stepwise reduction of Fenton reaction. Overwhelmed ROS can cause opening of the mitochondrial permeability transition pore (MPTP) which irreversibly damage the respiratory chain (Kalogeris *et al.*, 2014). Consequently, intrinsic antioxidant systems

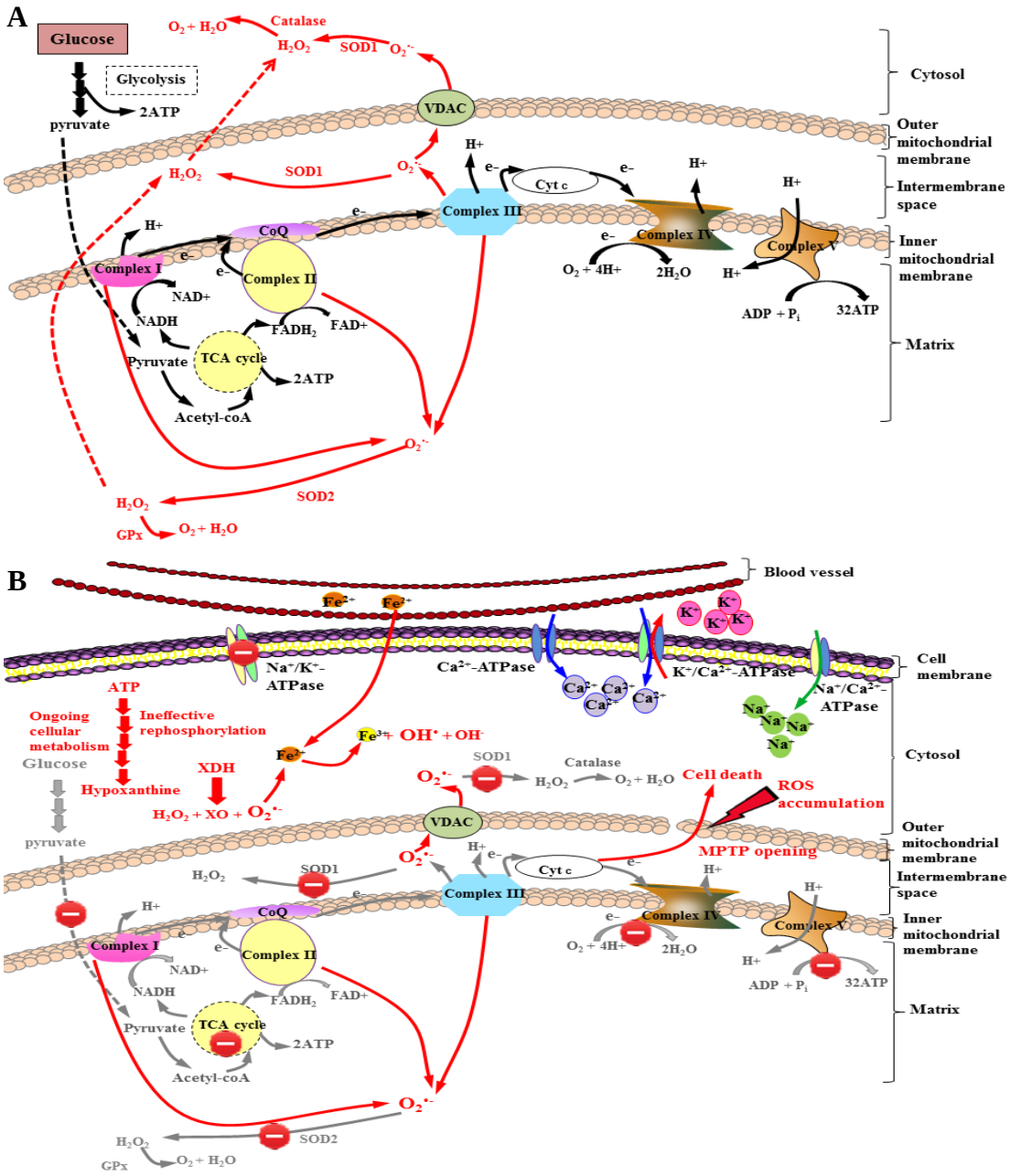

Figure 1.5 Schematic illustration of free radical production and scavenging under (A) physiological conditions and (B) after ischemic stroke as indicated in red. (A) Under normal conditions, complex I, II and III release $O_2^{\bullet-}$ as byproduct of ETC. Intrinsic antioxidant systems such as SOD1 and SOD2 convert $O_2^{\bullet-}$ into H_2O_2 and water. Then, catalase and GPx convert H_2O_2 into oxygen and water. Thus, ROS is maintained at low levels. (B) Under ischemia, impaired oxygen and glucose supplies cause ATP depletion. Consequently, ATP is degraded to hypoxanthine. Ca^{2+} influx activates Ca^{2+}-dependent proteases which convert XDH to XO, $O_2^{\bullet-}$ and H_2O_2. Due to oxygen deprivation, XO is unable to convert hypoxanthine to xanthine. H_2O_2 is partially reduced to highly reactive $^{\bullet}OH$. Degraded heme proteins release Fe^{2+} which react with H_2O_2 to form highly reactive $^{\bullet}OH$. ROS accumulation leads to opening of MPTP, Cyt c release, irreversible damage of the respiratory chain, mitochondrial dysfunction and cell death. Figure is generated using Cell Illustrator 5 and Microsoft PowerPoint.

are unable to counterbalance the free radical production. The free radicals oxidize the DNA, protein and lipids, which lead to mitochondrial dysfunction and cell death.

1.1.2 Reperfusion injury

During reperfusion, blood supply returns to the ischemic tissue. The reintroduction of oxygen activates XO that has accumulated during ischemia (Granger and Kvietys, 2015). XO catalyzes conversion of hypoxanthine that has built up during ischemia to form xanthine. Xanthine is subsequently oxidized by XO to form uric acid. $O_2^{\bullet-}$ and H_2O_2 are produced as byproducts of both oxidation processess. H_2O_2 can be converted to highly destructive $^{\bullet}OH$ by Fe^{2+}-mediated Fenton reaction and Harber-Weiss reaction (Das *et al.*, 2014). As a consequence, the intrinsic antioxidant defence systems are overwhelmed by the rapid generation of $O_2^{\bullet-}$ and $^{\bullet}OH$ which exacerbate the oxidative stress induced by ischemia. Besides, reperfusion also accelerates the neutrophil infiltration and pro-inflammatory mediators release (Schofield *et al.*, 2013). Neutrophils consist of nicotinamide dinucleotide phosphate (NADPH) oxidase then reduces the oxygen to $O_2^{\bullet-}$. Hence, neutrophil activation aggravates ROS formation in the reperfused tissue (Schofield *et al.*, 2013). The inflammatory response also causes endothelial and parenchymal cell damage. Thus, reperfusion extends the ischemia-induced injuries, triggering more severe cascades of cell death.

1.1.3 Current treatment for stroke

The only US Food and Drug Administration (FDA)-approved thrombolytic drug to treat ischemic stroke is recombinant tissue plasminogen activator (r-tPA) (Roth, 2011). It is a clot busting drug that must be given to patients within 4.5 h after

stroke onset to restore the blood flow (Roth, 2011). Besides, r-tPA is only eligible for patients age 18-80 years old without prior history of both stroke and diabetes and not under oral anticoagulants prescription (Demaerschalk *et al.,* 2015). Delayed r-tPA administration after 4.5 h could lead to dentrimental side effects such as intracerebral hemorrhagic transformation (HT) and blood brain barrier (BBB) rupture which contributes to high morbidity in patients (Wang *et al.,* 2015). r-tPA cleaves the zymogen plasminogen to form activated plasmin which degrades the fibrin clot (Chevilley *et al.,* 2015).

Neuroendovascular procedures can be done within 6 h of first stroke symptoms and only after r-tPA administration provide better outcomes in patients (Asil and Gultekin, 2016). During neuroendovascular procedures, a catheter is passed through the groin and navigated to the site of artery occlusion. The clot is then removed by the retrievable catheter. The narrow therapeutic window and strict eligibility criterias greatly impede effectiveness of treatment for majority ischemic stroke patients. Furthermore, none of these treatments have been successfully reversing the effect of ischemic stroke by regenerating new cells to replace the damaged brain tissue. As a consequence, stroke patients are usually associated with poor prognosis and high recurrent rate of stroke.

1.1.4 Stem cell therapy

Since last few years, stem cell therapy has been the most encouraging approach for treating neurodegenerative diseases and stroke (Lunn *et al.*, 2011; Kim *et al.,* 2013; Kumar *et al.*, 2016). The transplanted cells may help to create new circuitry and express factors that protect existing cells (De Feo *et al.,* 2012). Neural stem cells

(NSCs) are considered as the most optimal cell type for stem cell-mediated therapy of brain disorders such as stroke (Kim *et al.*, 2013). This is because they share the same tissue origin of the damaged brain cells and are originally meant to replenish the brain cells *in vivo*. In human brain, NSCs reside in two high-density cell division sites, the subventricular zone (SVZ) and subgranullar zone (SGZ) (Figure 1.6) (Gonzalez-Perez, 2012). NSCs are self renewal and able to differentiate into neuron, astrocyte and oligodendrocyte. They also have a lower oncogenic potential and immunological rejection (De Feo *et al.*, 2012). Thus, NSCs provide the great potential for clinical applications.

NSC transplantation has been studied in ischemic stroke animal models and human trial (Englund *et al.*, 2002; Kelly *et al.*, 2004; Date *et al.*, 2006; Jin *et al.*, 2011; Zhang *et al.*, 2011; Muir and Sinden, 2015). Transplanted NSCs have been reported to contribute for neuroprotective effects in ischemic stroke. Several studies have demonstrated that transplanted NSCs could migrate to the ischemic areas, differentiate into mature neurons and even promote endogenous neurogenesis (Jin *et al.*, 2011; Zhang *et al.*, 2011; Mine *et al.*, 2013). Besides, transplanted NSCs could ameliorate cerebral inflammation by reducing macrophage infiltration (Lee *et al.*, 2008). Transplanted NSCs also promote angiogenesis at surrounding infarcted region through release of paracrine factors such as vascular endothelial growth factor A (VEGFA), angiopoietin-1 (ANGPT1), epidermal growth factor (EGF) and basic fibroblast growth factor (bFGF) (Hicks *et al.*, 2013). Furthermore, Zhao and Wang (2013) demonstrated the anti-apoptotic effects of transplanted NSCs through enhanced mitogen-activated protein kinase/extracellular receptor kinase (MAPK/ERK) signaling in ischemic brain.

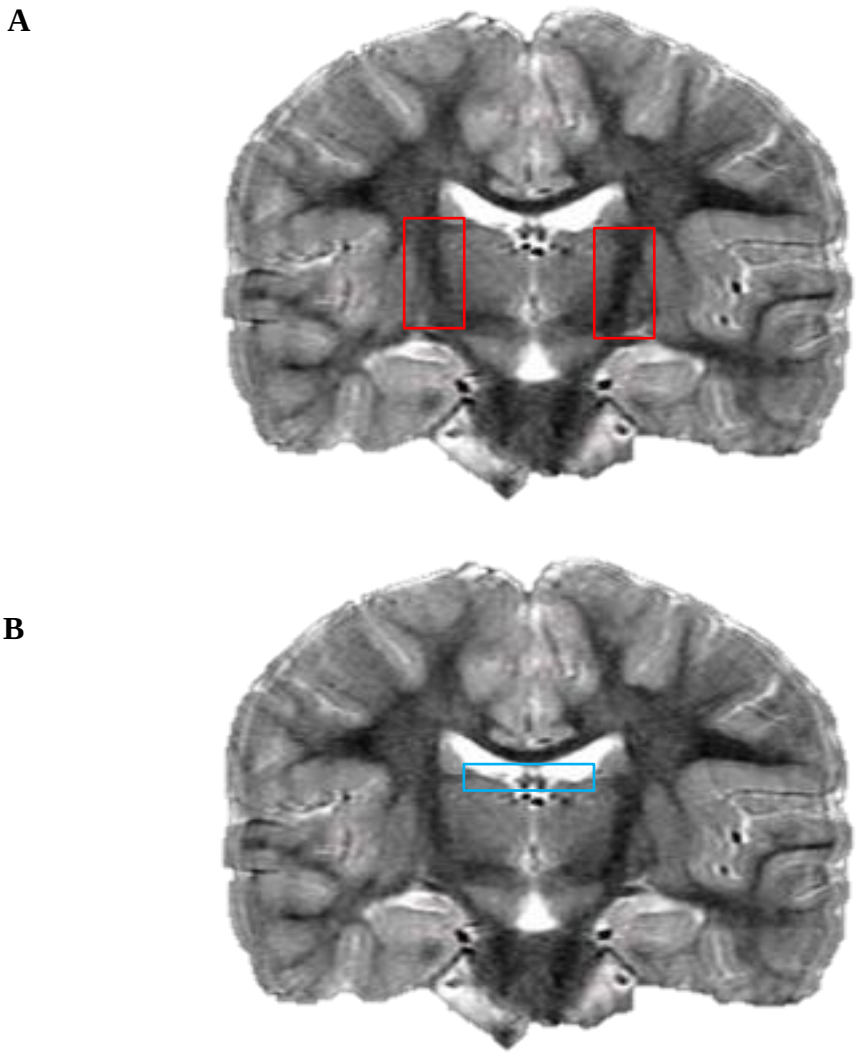

Figure 1.6 Coronal section of human adult brain. (A) NSCs reside within SVZ of the lateral ventricle (red boxes). (B) In adult hippocampus, NSCs are located in the SGZ of the dentate gyrus (blue box). Adapted from DeFelipe (2011).

Despite the great therapeutic potential of NSCs for ischemic stroke, the survival of grafted cells within the infarcted area remains a serious concern for NSC transplantation. This is because the ischemic/reperfused region is very harsh for cell survival due to the excessive free radicals, glutamate excitotoxicity and inflammation. As little as 0.09% retention rate of grafted cells were observed in mice with transient middle cerebral artery occlusion (MCAO) (Bacigaluppi *et al.*, 2009). Low cell survival rate limits the capacity of NSCs to repair the injured area and this poses a much more difficult challenge to the NSC-based therapy for ischemic stroke. To circumvent this problem, preconditioning of NSCs was employed.

1.2 Preconditioning strategy

The concept of preconditioning was first described in the past 30 years, whereby one or more brief episodes of sub-lethal stimuli was introduced to render the endogenous protective mechanisms against subsequent lethal injury (Murry *et al.*, 1986). Preconditioning can be achieved through physiological sub-lethal stimuli such as hypoxia, heat shock and carbon monoxide (Sharp *et al.*, 2004; Harder *et al.*, 2005; Vieira *et al.*, 2008). Besides, preconditioning can also be achieved through pharmacological agents such as minocycline, doxycycline, sevoflurane, cobalt chloride, baicalein and aromatic-tumerone (Wang *et al.*, 2010a; Sakata *et al.*, 2012; Wang *et al.*, 2012; Chang *et al.*, 2013; Dai *et al.*, 2014; Hucklenbroich *et al.*, 2014). This study focused on physiological and pharmacological preconditioning of NSCs using hypoxia and baicalein-enriched fraction from *Oroxylum indicum*, respectively.

1.2.1 Hypoxic preconditioning

Hypoxic preconditioning involves brief periods of hypoxia that triggers various protective signaling pathways and enhances resilience to ischemia (Sharp *et al.*, 2004; Wei *et al.*, 2017). Transcriptional responses to hypoxia are mediated by the hypoxia-inducible factor (HIF) (Sharp *et al.*, 2004). Under hypoxia, activated HIF binds to hypoxia response elements (HREs) and subsequently activates expression of target genes involved in angiogenesis, energy metabolism and cell proliferation. Hypoxic preconditioning has been shown to promote NSC survival after transplantation into ischemic rat brain (Wakai *et al.*, 2016).

Besides, previous studies had reported that NSC microenvironment is hypoxic by nature, whereby the oxygen level in the brain may be as low as 2% (Studer *et al.*, 2000). Thus, *in vitro* cultivation of NSCs in a typical incubator condition of 21% oxygen does not reflect the physiologic norms. The normoxic condition is unlikely to be optimal for maintaining normal proliferative state of NSCs (Studer *et al.*, 2000). Several studies have demonstrated that priming the endogenous NSCs using hypoxic preconditioning method can enhance the cell proliferation and differentiation in animal models (Giese *et al.*, 2010; Wakai *et al.*, 2016).

1.2.2 Pharmacological preconditioning by baicalein-enriched fraction

Pharmacological preconditioning involves brief periods of exposure to pharmacological agents that triggers intrinsic protective mechanisms and enhances resilience to subsequent lethal insults (Gidday, 2010). Baicalein (5,6,7 trihydroxyflavone) is a flavonoid aglycan derived from *Scutellaria baicalensis* and *Oroxylum indicum* (Majeed et al., 2017). Like many flavonoid compounds,

baicalein can exert both antioxidant and pro-oxidant effects depending on cell types (Woo *et al.*, 2005; Kang *et al.*, 2012). Spectroscopic scanning measurements by Cho *et al.* (2008) revealed the binding of baicalein to prolyl hydroxylase 2 (PHD2) and factor inhibiting HIF-1 (FIH-1) under normoxia. Baicalein was found to compete with 2-oxoglutarate (2OG) for the active sites of PHD2 and FIH-1 through its 3-hydroxyl structure. Hence, baicalein abrogated hydroxylation of hypoxia-inducible factor-1 alpha (HIF-1α) similar to those observed in hypoxic preconditioning. In addition, Chang *et al.* (2013) demonstrated that pharmacological pretreatment of chick cardiomyocytes using baicalein derived from *S. baicalensis* for 10 min prior to ischemia/reperfusion mediated a pro-oxidant preconditioning effects which mimicks hypoxic preconditioning. Consequently, pre-treatment with baicalein confered cytoprotection against ischemia and reperfusion injury in those cardiomyocytes and reduced apoptosis (Chang *et al.*, 2013). The effects of baicalein on NSC have not been determined previously. Baicalein has been described to exert anti-proliferative and pro-proliferative activity depending on cell types. Baicalein treatment was found to attenuate proliferation of numerous human cancer cell lines (Cathcart *et al*., 2016; Bie *et al*., 2017; Zhou *et al*., 2017). However, it promoted proliferation in hematopoietic stem cells (Patwardhan *et al.*, 2014). Hence, it is crucial to determine the effects of baicalein-enriched fraction particularly on NSCs.

1.2.2(a) Baicalein-enriched fraction from *Oroxylum indicum*

Considering the promising neuroprotection potentials of baicalein, this study sought to produce an enriched baicalein fraction from the leaves of *O. indicum* as pharmacological agent for preconditioning. Besides *O. indicum* leaves, baicalein is also the major constituent in the roots of *S. baicalensis* (Aliev *et al.*, 2014). However,

S. baicalensis requires destructive harvest which may lead to severe depletion of medicinal plant resources (Nishteswar, 2014). Hence, in this study, *O. indicum* leaves offer better resources without the removal of entire plant.

Briefly, *O. indicum* is a medicinal herb belongs to family of Bignoniaceae that is commonly found in many regions of South-east Asia (Harminder *et al.*, 2011). It is a deciduous soft wooded tree with pinnately compound, ovate-elliptic leaves and acuminate leaf tips (Figure 1.7A and B) (Harminder *et al.*, 2011). This tree also has large flowers with stinky odour that bloom at night time to attract pollinators (Figure 1.7C). It also has long and flattened fruit pods that hang down from the thick branches like dangling swords (Figure 1.7D). When the pod burst, the flat and semi-transparent winged seeds flutter like butterflies (Figure 1.7E). Hence, the seeds are known as "mu hu die" (tree butterfly) in Chinese herbal medicine (Chen *et al.*, 2003b). In Malaysia, it is commonly known as "Beko" and the young leaves as well as fruits are consumed raw as salad by the local community. Different parts of *O. indicum* such as fruits, root barks and leaves have been applied in traditional medicine to treat bronchitis, dyspepsia, asthma, gastropathy, inflammation and microbial infection (Harminder *et al.*, 2011). Preconditioning by baicalein-enriched fraction is also postulated to trigger similar neuroprotective mechanisms induced by hypoxic preconditioning.

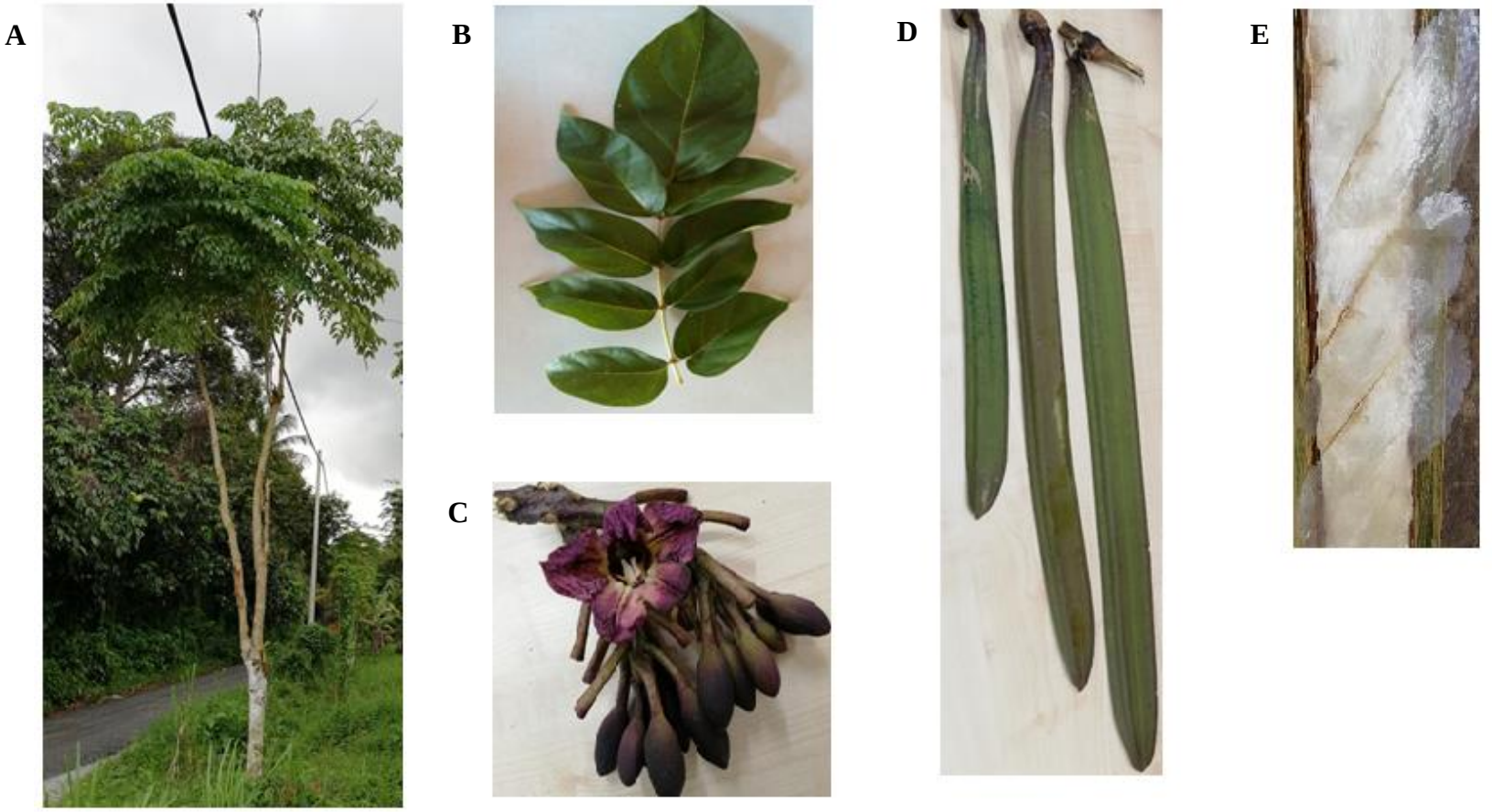

Figure 1.7 Representative images of *O. indicum*. (A) *O. indicum* is a medium-sized tree that branched at top. (B) The leaves are pinnately compound, ovate-elliptic with acuminate tips. (C) The flower emits strong and stinky smell to attract night pollinators. (D) Long and flattened fruit pods that hang down from the thick branches like dangling swords. (E) The seeds are flat with semi-transparent wings. Pictures of plants were taken during botanical field trip for plant specimen collection.

1.2.3 Preconditioning-induced neuroprotective signaling

Physiological and pharmacological preconditioning have been reported to enhance resistance to lethal insults through activation of endogenous survival cascades such as HIF-1α, neurogenic locus notch homolog protein 1 (Notch 1), VEGFA, ANGPT1, nuclear factor erythroid 2-related factor 2 (Nrf2) and SOD1 (Figure 1.8) (Chen *et al.*, 2003a; Belaidi *et al.*, 2006; Stubbs *et al.*, 2012; Zhou *et al.*, 2013; Huang *et al.*, 2014).

1.2.3(a) Hypoxia-inducible factor-1 alpha (HIF-1α)

HIF-1 is a basic Helix-Loop-Helix-Period-Arnt-Single minded-homology (bHLH-PAS) domain transcription factor composed of an alpha (α) and a beta (β) subunit (Semenza *et al.*, 1997). The oxygen-labile α subunits consisted of HIF-1α, HIF-2α and HIF-3α wherease β subunit, HIF-1β, is constitutively presented in the nucleus (Semenza *et al.*, 1997). Apart from bHLH-PAS domain, HIF-1α also comprises of transactivation domains (TAD) and oxygen-dependent degradation domain (ODD) as shown in Figure 1.9A (Semenza *et al.*, 1997).

HIF-1α expression is regulated by PHD2 and FIH-1. Under normoxic conditions, PHD2 catalyzes hydroxylation of two highly conserved proline residues (Pro402 and Pro564) within the ODD of HIF-1α (Figure 1.9B). The enzymatic process utilizes Fe^{2+} as co-factor whilst oxygen and 2OG as substrates. An E3 ubiquitin ligase complex known as von Hippel-Lindau (pVHL) further targets the hydroxylated HIF-1α for proteasomal degradation. In addition, FIH-1 catalyzes hydroxylation of asparagine residue (Asn803) within the C-TAD of HIF-1α (Figure 1.9C). Similar to PHD2, the hydroxylation requires Fe^{2+} as co-factor whilst oxygen and 2OG as

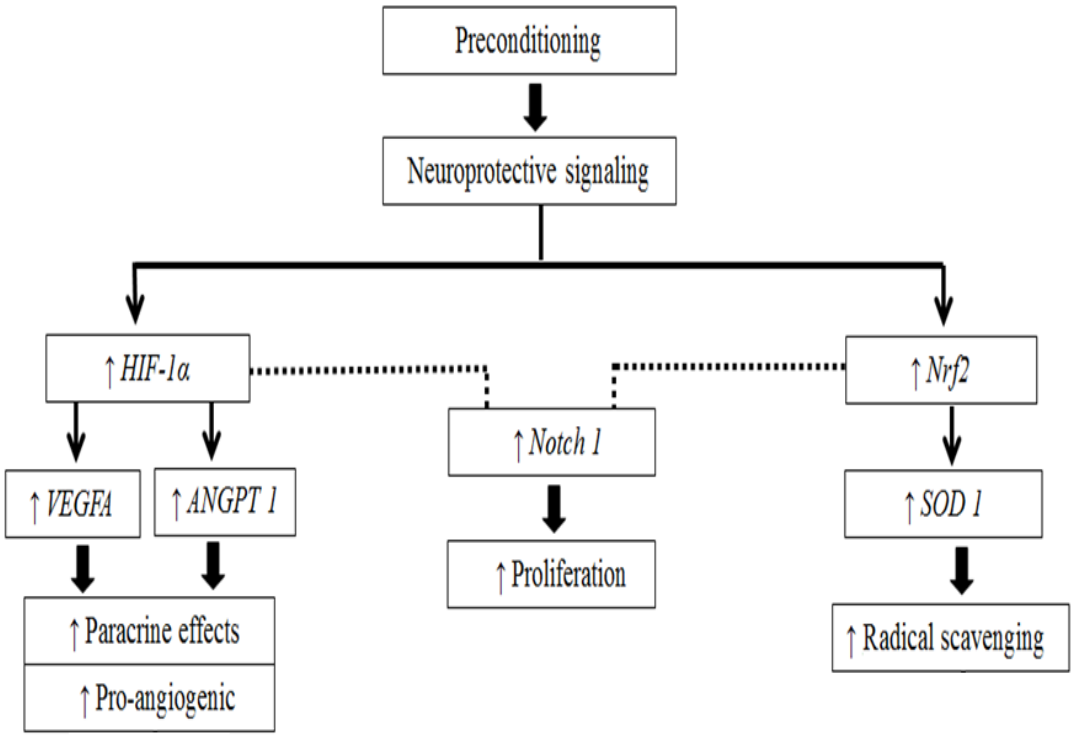

Figure 1.8 Preconditioning-induced neuroprotective signaling. Preconditioning modulated adaptive and recuperative mechanisms through HIF-1α, Notch 1, VEGFA, ANGPT1, Nrf2 and SOD1. HIF-1α enhanced VEGFA and ANGPT1 signaling to stimulate paracrine effects and angiogenesis whereas Nrf2-mediated SOD1 expression stimulates free radical scavenging. The crosstalk of HIF-1α and Nrf2 with Notch 1 promotes cell proliferation.

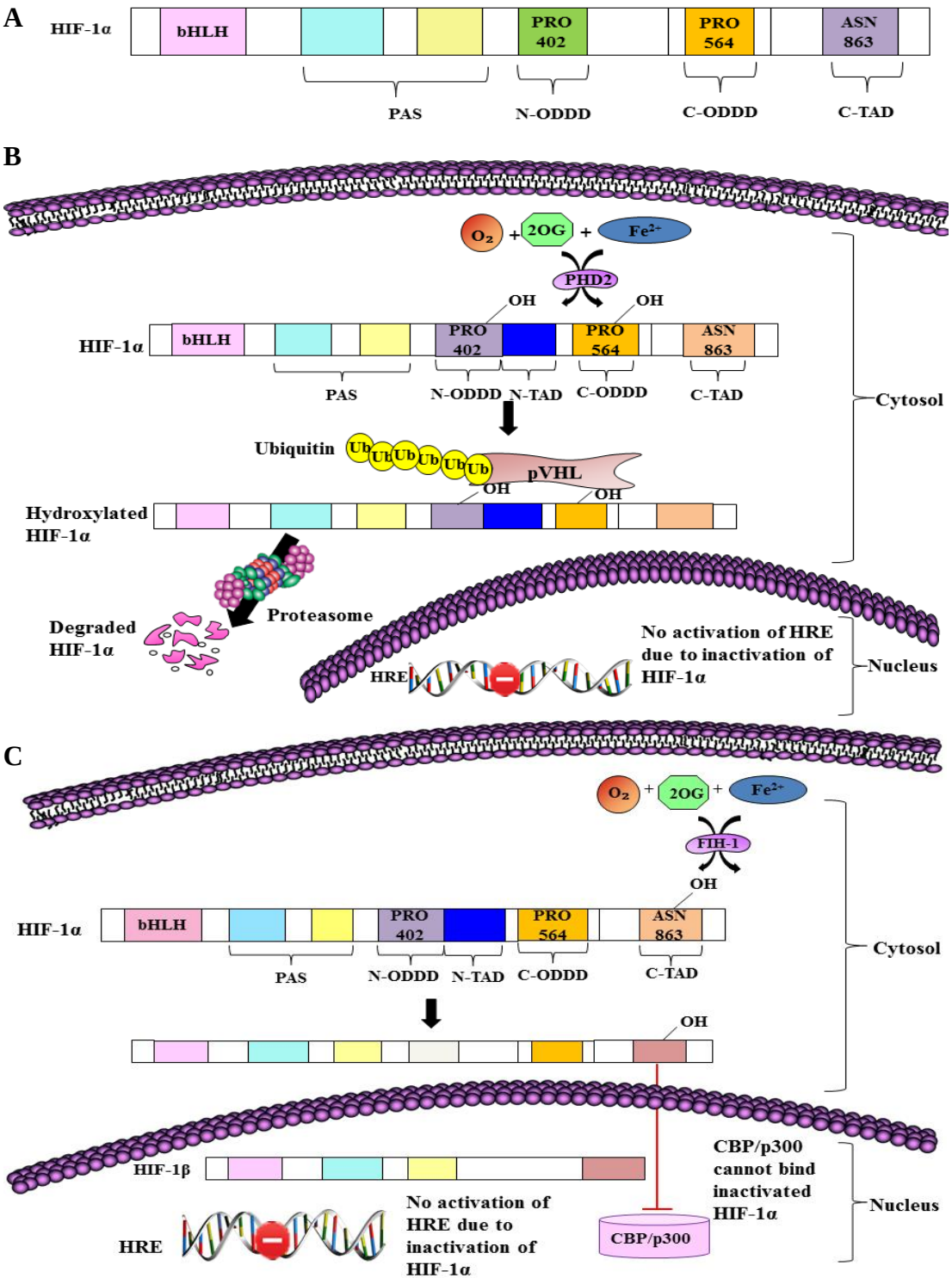

Figure 1.9 Schema illustrating (A) HIF-1α domain structure, (B) PHD2 and (C) FIH-1 regulated HIF-1α degradation under normoxic conditions. (A) HIF-1α contain bHLH-PAS, TAD and ODDD. (B) Using oxygen, 2OG and Fe^{2+}, HIF-1α is degraded by PHD2 signaling. (C) FIH-1 also catalyzes hydroxylation of HIF-1α in the presence of oxygen, 2OG and Fe^{2+}. Hydroxylated HIF-1α could not bind to CBP/p300 for downstream HIF-1α target genes. Hence, transcriptional activity of HIF-1α is inhibited (Masson and Ratcliffe, 2003). Figure is generated using Cell Illustrator 5 and Microsoft PowerPoint.